# Supplementary material for "A New Method to Study the Change of miRNA-mRNA Interactions Due to Environmental Exposures"

Francesca Petralia[1], Vasily Aushev[2], Kalpana Gopalakrishnan[2], Maya Kappil[2], Nyan Win Khin[2], Susan Teitelbaum[2], Jia Chen[2], and Pei Wang[1]

[1]Department of Genetics and Genomic Sciences, Icahn School of Medicine at Mount Sinai, 1425 Madison Avenue, New York, NY 10029, USA
[2]Department of Environmental Medicine and Public Health, Icahn School of Medicine at Mount Sinai, 1 Gustave Levy Place, Box 1057, New York, NY 10029, USA

## Contents



## 1 Importance score cut-off

Let $I^g_{j\to k}$ be the importance score corresponding to the interaction event $(j \to k)$ between miRNA $j$ and gene $k$ in the $g$th tree ensemble. Specifically, this importance score is defined as $I^g_{j\to k} = \frac{1}{T}\sum_{\tau\in\mathcal{N}_{gj}} C^\tau_{gj}$ where $T$ is the number of random forest trees, $\mathcal{N}_{gj}$ is the set of nodes which utilize the $j$th miRNA for the splitting rule in the $g$th tree ensemble and $C^\tau_{gj}$ is the decrease in node impurity observed in the $g$th random forest model after splitting $\tau$ based on the $j$th predictor. In order to derive the final unweighted networks, a proper cut-off value for importance scores $\{I^g_{j\to k}\}_{j=1}^M$ needs to be chosen. In particular, we utilize the following permutation based procedure which derives the density of importance score under the assumption of no interaction (Petralia *et al.*, 2016).

(a) For $b \in \{1, \cdots, B\}$, with $B$ being the number of permutations,

(a.1) Randomly permute the sample order of the expression of the target gene (response variable) for each data type $g \in \{1, \ldots, G\}$, i.e., permute values in vector $\mathbf{y}_k^g = \{y_{1k}^g, \ldots, y_{n_g k}^g\}$. Fit $G$ random forest models (one for each treatment condition) via iJRF to predict the expression of the target gene based on the expression of miRNAs.

(a.2) Compute the final importance scores for relationships $\{m \to k\}_{m=1}^M$ in each class $g$ which are denoted as $\{I_{m\to k}^{g,b}\}_{m=1}^M$.

(b) For each class $g$ and threshold $\iota$, we compute

$$f_g(\iota) = \frac{\frac{1}{B}\sum_{b=1}^B \sum_{m=1}^M \mathbf{1}(I_{m\to k}^{g,b} > \iota)}{\sum_{m=1}^M \mathbf{1}(I_{m\to k}^{g} > \iota)}$$

where $\mathbf{1}(A)$ is the indicator function, equal to one if event $A$ occurs and zero otherwise.

$f_g(\iota)$ can serve as an approximation of the false discovery rate (FDR) (Tusher *et al.*, 2001). In our application, we use $B = 200$ and $\iota_0^g = \min\{\iota : f_g(\iota) \leq 0.001\}$ and declare an edge between $j$ and $k$ in class $g$ if $I_{j\to k}^g > \iota_0^g$.

# 2 Inferred Networks

## 2.1 Computational Time

In this section, we provide some information about the computational time needed to run iJRF for our particular data application. As mentioned in section 2.2 of the main manuscript, iJRF's computational complexity is $O(pTN\sum_{g=1}^G \log(n_g)n_g)$ wth $p$ being the number of mRNAs, $N$ the number of predictors (miRNAs) sampled at each node, $T$ the number of random forest trees and $n_g$ the sample size of the $g$th data set. In practice, iJRF analysis can be completed for all $7,546$ target genes in about 56 minutes using an Intel 2 core machine. When the job is run on a server using parallel computing, the analysis can be performed within a few minutes. In fact, the computational time of running iJRF for 100 target genes using an intel 2 core machine is about 45 seconds.

## 2.2 Chemical Networks

In this section, we provide more details on chemical networks, i.e., DEP-Net, MPB-Net and TCS-Net. In particular, DEP-Net contained $3,018$ interactions linking 47 miRNAs and $1,311$ mRNAs; MPB-Net $5,743$ interactions linking 57 miRNAs and $2,119$ mRNAs; while TCS-Net contained $3,557$ interactions linking 50 miRNAs and $1,385$ mRNAs. Therefore, DEP was the chemical with the smallest number of estimated miRNA-mRNA interactions. In addition, a substantial portion ($> 68\%$) of the interactions contained in DEP-Net were present in Control-Net. Figure S1 shows the top 10 miRNAs in chemical-networks that were responsible for more than 90%, 88% and 87% of the interactions in DEP-Net, MPB-Net and TCS-Net, respectively. For each miRNA, Figure S1 shows, the number of edges shared between chemical-Net and Control-Net (green bar), the number of control-specific edges (blue bar) and the number of chemical-specific edges (red bar). The three quantities have been normalized dividing them by the total number of connecting edges present in either control or chemical-networks. Although Control-Net has more interactions than chemical-networks, there are some interesting miRNAs more connected in chemicals rather than in control. As an example, miR-205 is connected to 103 mRNAs in DEP-Net, 283 mRNAs in MPB-Net, 181 mRNAs in TCS-Net, while only to 137 mRNAs in Control-Net. Another interesting miRNA is miR-29a-3p which is more connected in chemicals (DEP: 90 edges, MPB: 99 edges and TCS: 100 edges) than in control (58 edges). These miRNAs are already known in breast cancer literature (Cai *et al.*, 2016; Das and Lin, 2016; Li *et al.*, 2016a; Zhang *et al.*, 2015) for their role in drug sensitivity and diagnosis.

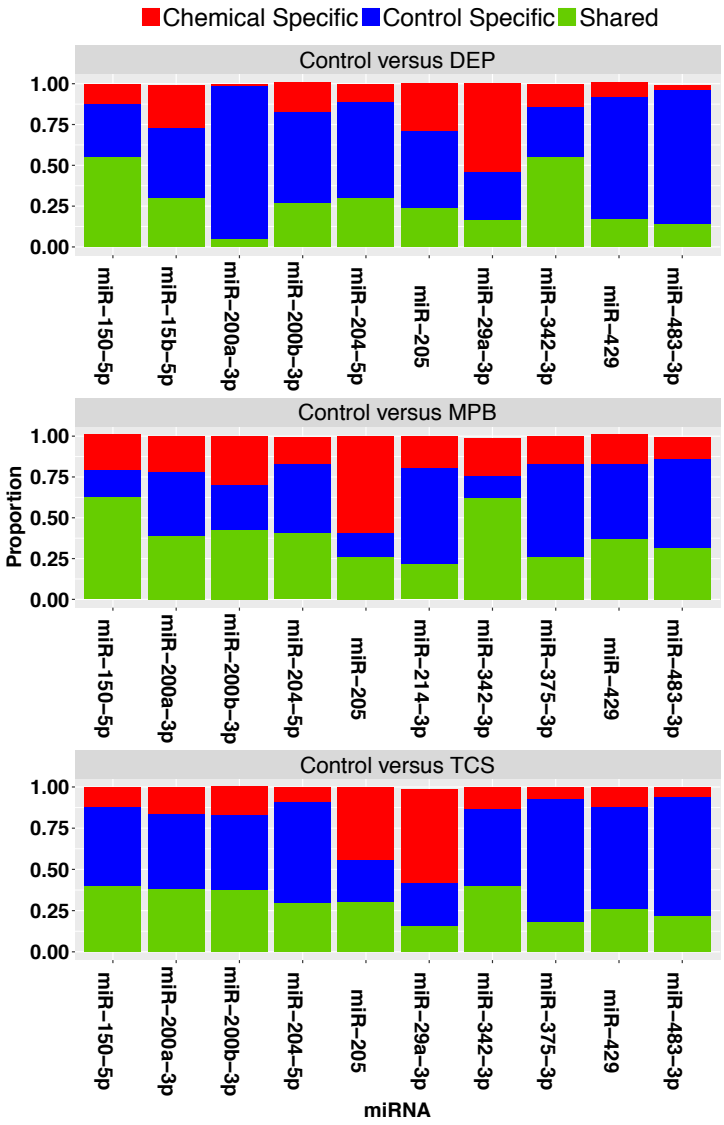


**Figure S1.** Top 10 miRNAs in DEP-Net, MPB-Net and TCS-Net. These miRNAs are responsible for more than 85% of the interactions in chemical networks. For each miRNA, we show the number of edges shared between chemical-Net and Control-Net (green bar), the number of control-specific edges (blue bar) and the number of chemical-specific edges (red bar). The three quantities have been normalized dividing them by the total number of connecting edges present in either control or chemical-networks.

Figure S2 provides a pairwise comparison between chemical networks, i.e., DEP vs MPB, DEP vs TCS and MPB vs TCS. For each pairwise comparison, we show miRNAs with more than 20 connecting edges in at least one of the two networks compared.

*DEP versus other chemicals* Despite the loss of interactions observed in DEP-Net, some miRNAs such as miR-15b-5p, miR-183-5p and miR-146a-5p are higher connected in DEP-Net compared to MPB-Net and TCS-Net. These three chemicals should be considered for further investigations. As shown in Figure S2, miR-375 and miR-200a are the two miRNAs where the most dramatic loss of interaction is observed in DEP-Net compared to MPB-Net and TCS-Net. These two miRNAs were experimentally validated in our study given the loss of interactions observed in DEP-Net compared to Control-Net.

*MPB versus other chemicals* Few miRNAs such as miR-672-5p, miR-146a-5p, miR-15b-5p, miR-181a-5p and miR-199a-5p are higher connected in MPB-Net compared to TCS-Net. Among these miRNAs, miR-199a-5p is the one with the highest number of connecting edges in MPB-Net (MPB: 70 edges, TCS: 26 edges). The number of connecting edges of miR-199a-5p in Control-Net is instead 23 and, therefore, miR-199a-5p can be considered as MPB-specific hub miRNA. miR-199a-5p has been linked to breast cancer in different studies (Chen *et al.*, 2016; Li *et al.*, 2016b; Yi *et al.*, 2013) and Shin *et al.* (2015) suggested a role as triple negative breast cancer marker with diagnostic value. Further analyses are necessary to elucidate the effect of MPB on the regulatory mechanisms of miR-199a-5p.

*TCS versus other chemicals* Compared to DEP-Net, TCS-Net involves a much higher number of connecting edges for miR-375-3p and miR-200a-3p. However, as shown in Figure S1, a loss of interactions is observed in TCS-Net compared to Control-Net, and threfore cannot be considered a TCS-specific hub-miRNA. In the comparison of TCS-Net with MPB-Net, particularly interesting is miR-497-5p that is connected to 30 mRNAs in TCS-Net while only to 7 mRNAs in MPB-Net. Again, this miRNA was more connected in Control-Net (45 edges) than TCS-Net and, therefore, cannot be considered a TCS-specific hub-miRNA.

# 3 Other methods

## 3.1 Marginal Analysis

No significant results were detected by traditional univariate analysis (i.e., t-test, Wilcoxon test) testing the difference in expression of miRNAs between Control and treatment groups. As an example, for each miRNA, we tested the difference in expression between control and each treatment (i.e., DEP, MPB and TCS) using the unpaired Wilcoxon test. The Wilcoxon test was chosen over a t-test given the small sample size of the study. Figure S3 shows the distribution of p-values on a $-\log_{10}$ scale. It is important to notice that these p-values were not adjusted for multiple comparison and no p-value was significant ($< 0.20$) after Benjamini correction.

## 3.2 miRNA-mRNA Interactions via Correlation Test

For each chemical treatment and control, we inferred miRNA-mRNA interactions using Pearson's correlation test. Specifically, for each miRNA-mRNA pair and one treatment condition, an edge is declared between the pair if their correlation under the treatment condition is significant after adjusting for multiple comparison. The following paragraphs contain results for two different false discovery rate (FDR) cut-off, i.e., fdr $= 0.01$ and fdr $= 0.001$.

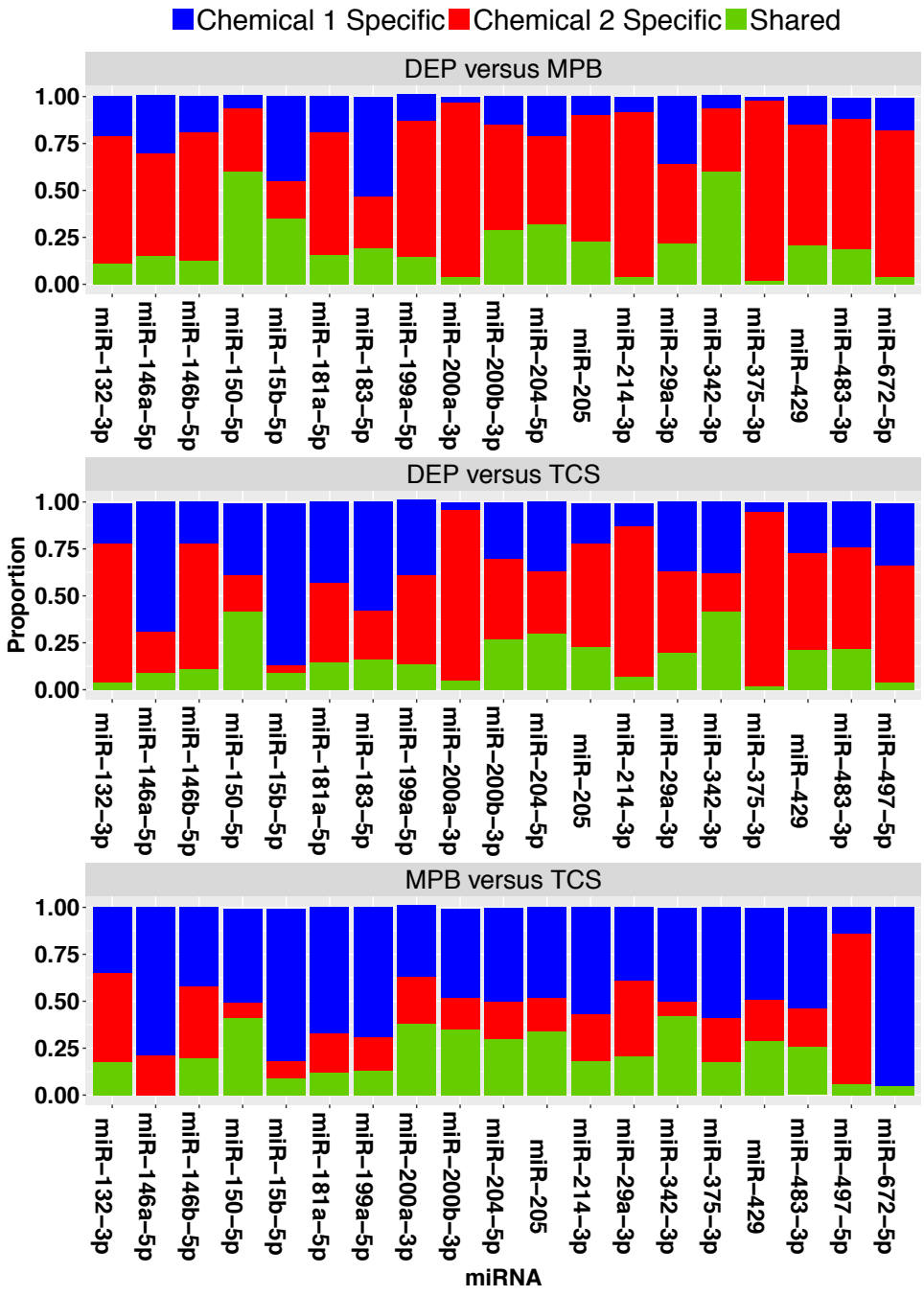


**Figure S2.** Pairwise comparison between chemical networks. For each pairwise comparison, we show only miRNAs with more than 20 edges in at least one of the two chemical networks compared. For each miRNA, we show the number of edges shared between the two networks (green bar), the number of chemical 1 specific edges (blue bar) and the number of chemical 2 specific edges (red bar). The three quantities have been normalized dividing them by the total number of connecting edges present in at least one of the two networks compared.

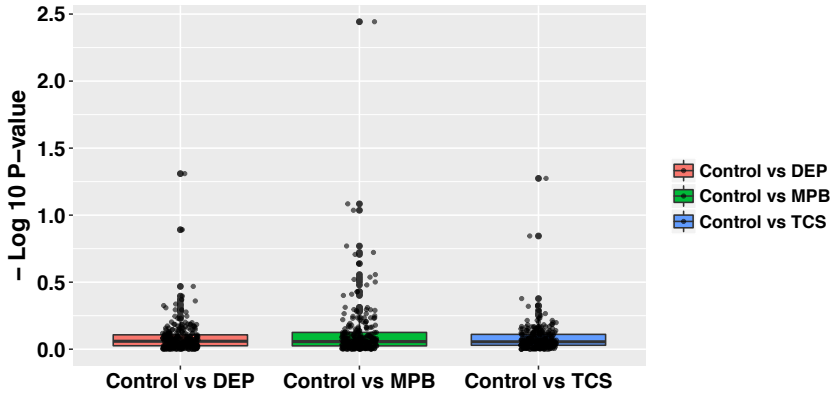


**Figure S3.** Pvalues (- log 10 scale) from unpaired Wilcoxon test comparing the difference of miRNA expression between Control and chemical treatment.

**FDR cut-off 0.001** In order to derive miRNA-mRNA networks from iJRF, an FDR cut-off of 0.001 was considered (see section 1 of supplementary material). Such stringent cut-off is generally utilized for high-dimensional data applications. Table S1 shows the number of edges detected by the correlation test using the same FDR cut-off. Consistently with iJRF's results, a loss of connectivity is registered in chemicals compared to control. However, the number of detected edges is much lower than that of iJRF (see Table 1 in the main manuscript). In particular, more than 89% of the edges in Control-Net resulting from correlation test involve three top miRNAs, i.e., miR-375-3p, miR-483-3p and miR-150-5p, which are among the top 10 miRNAs detected by iJRF (see Figure 2 of the main manuscript). As shown by Figure S4, these top miRNAs play a limited role in chemical networks. Particularly interesting is miR-375-3p, one of the miRNAs experimentally validated in our study. Figure 3(a) in the main manuscript showed some interesting enriched pathways such as "Mammary Gland Development" and "Gland Morphogenesis" for mRNAs connected to miR-375-3p in Control-Net but not in DEP-Net. In the same way, we derived pathways enriched for mRNAs connected to miR-375-3p and miR-200a-3p in Control-Net but not in DEP-Net based on the correlation test. Unfortunately, no pathway was enriched using Benjamini's adjusted p-value of 0.01. Therefore, iJRF detected more associations and identified more interesting mechanisms compared to the correlation model.

**FDR cut-off 0.01** Table S1 shows the number of edges detected by the correlation test applying a cut-off of 0.01. Again, a loss of connectivity is registered in chemical networks compared to Control-Net. Figure S5 shows the degree plot of the top ten hub-miRNAs in Control-Net. Although the top 10 miRNAs detected by the correlation test and iJRF are mostly the same, the correlation model results in less overlapping networks compared to iJRF. As an example, only 6% of edges in DEP-Net are shared with Control-Net based on the correlation model, ten times less than the number of shared edges detected by iJRF (Table 1 in the main manuscript). This result is expected as iJRF, through joint learning, is more effective to detect common associations than algorithms handling different treatment conditions separately (Petralia *et al.*, 2016). Moreover, as demonstrated by Petralia *et al.* (2016), using random forest models to characterize interaction patterns is more powerful than a joint learning based on Gaussian graphic models (Danaher *et al.*, 2014).

To further compare our joint learning with the correlation test, an enrichment analysis was performed. Specifically, for each miRNA, we considered the set of connected messanger RNAs and derived the list of enriched GO terms. In particular, enrichment analysis was performed using David Tools (version 6.7) (Huang *et al.*, 2008) and only GO terms with Benjamini adjusted p-value less than 0.01 were considered

**Table S1.** Number of interactions inferred in Control-Net, DEP-Net, MPB-Net and TCS-Net with two different FDR cut-off, i.e., 0.001 and 0.01.

**FDR Cut-Off 0.001**

| | Control | DEP | MPB | TCS |
|---|---|---|---|---|
| Control | 287 | 0 | 1 | 0 |
| DEP | | 179 | 47 | 0 |
| MPB | | | 234 | 0 |
| TCS | | | | 6 |

**FDR Cut-Off 0.01**

| | Control | DEP | MPB | TCS |
|---|---|---|---|---|
| Control | 4,893 | 87 | 505 | 21 |
| DEP | | 1,352 | 456 | 1 |
| MPB | | | 2,926 | 10 |
| TCS | | | | 1,038 |

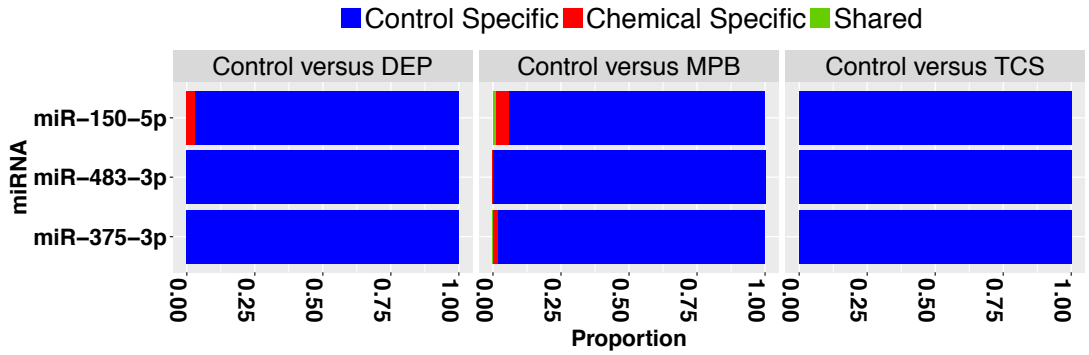


**Figure S4.** Degree plot for top-miRNAs resulting from correlation test applying an FDR cut-off of 0.001. For each miRNA, we show the number of edges shared by chemical and control (green bar), the number of control-specific edges (blue bar) and the number of chemical-specific edges (red bar). The three quantities have been normalized dividing them by the total number of connecting edges in either Control-Net or chemical networks.

as enriched. Figure S6 shows the total number of enriched GO terms resulting from both the correlation test and iJRF. As shown, for all networks, iJRF results in more enriched pathways than the correlation test. Therefore, despite using a less stringent FDR cut-off, the correlation test fails to reveal biological processes detected by iJRF.

# 4 MirTarBase

Table S2 shows the list of interactions for the 10 leading miRNAs in Control-Net contained in miRTarBase (Hsu *et al.*, 2010). As shown, some of the interactions are contained in DEP-Net, MPB-Net and TCS-Net as well.

# 5 Enrichment Analysis

Table S3 shows some of the enriched categories for the top leading miRNAs in Control-Net. For each miRNA $j$, we consider the list of genes connected to $j$ in Control-Net but not in chemical-networks and derived enriched GO terms using David Tools (Huang *et al.*, 2008). As shown, enriched GO terms include "Plasma Membrane", "Mammary Gland Development", "Immune Response" and "T-Cell Activation". Only enriched categories with p-values smaller than 0.01 are shown.

Figure S7(a) shows the density of the absolute value of correlation between miR-375-3p and miR-200a-3p with genes connected to them in Control-Net but not in DEP-Net. In Figure S7(b), we test the difference in correlation between Control and DEP groups for genes connected to miR-375-3p and miR-200a-3p only in Control. For this purpose, we consider the following statistics $\frac{\sum_{j=1}|\rho_{j,m}^{Control}|}{\sum_{j=1}|\rho_{j,m}^{dep}|}$ with $\rho_{j,m}^{h}$ being the correlation between gene $j$ and miRNA $m$ under $h$ treatment condition. Then, we permuted labels between Control and DEP category $1,000$ times and calculated the same statistics. The histogram in Figure S7(b) shows the value of the statistics over $1,000$ permutations. As shown, the true value (solid red line) is in the tail of the null density (p-values equal to 0.028 and 0.06 for miR-375-3p and miR-200a-3p, respectively) indicating that the loss of correlation observed under DEP exposure is significant.

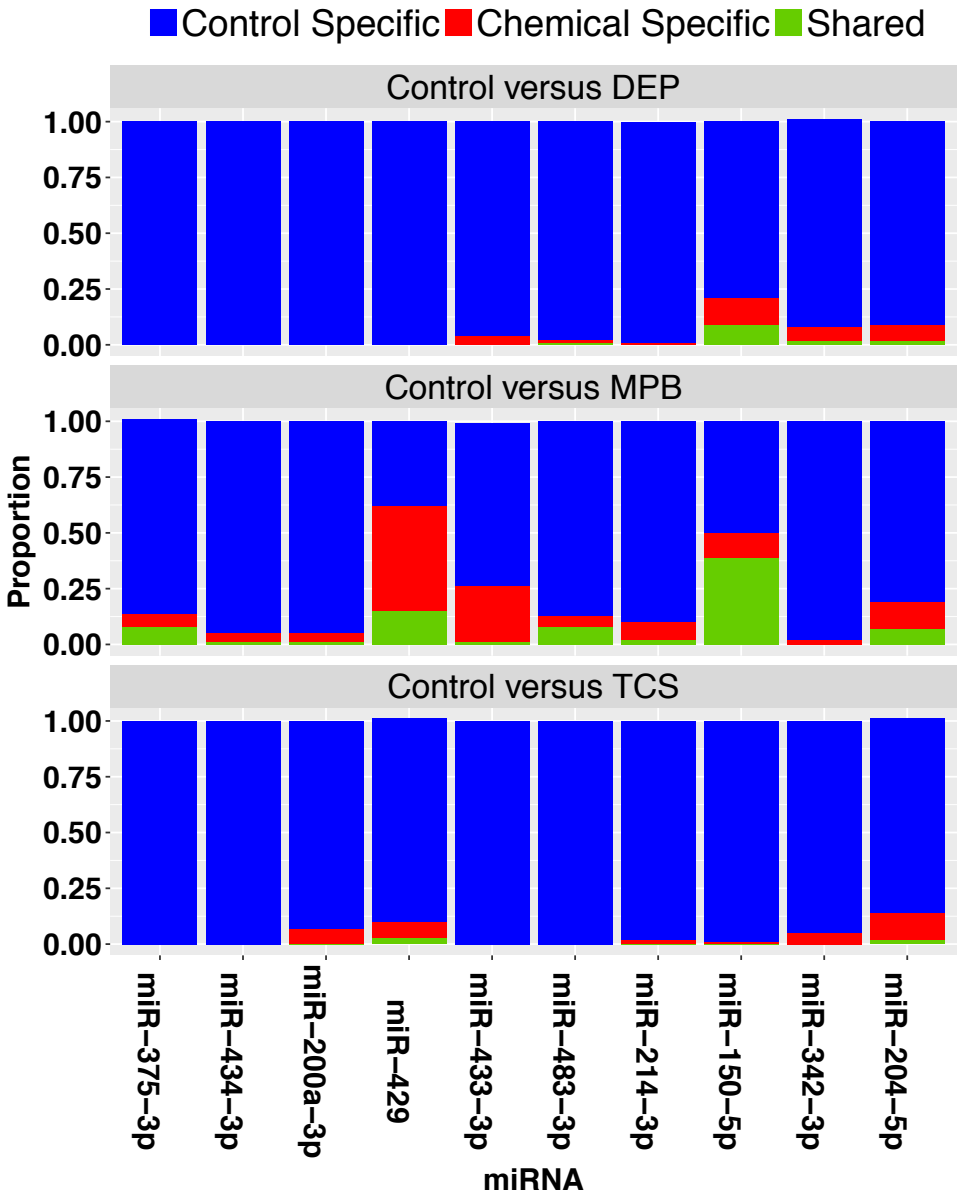


**Figure S5.** Degree plot for top-miRNAs resulting from correlation test applying an FDR cut-off of 0.01. For each miRNA, we show the number of edges shared by chemical and control (green bar), the number of control-specific edges (blue bar) and the number of chemical-specific edges (red bar). The three quantities have been normalized dividing them by the total number of connecting edges in either Control-Net or chemical networks.

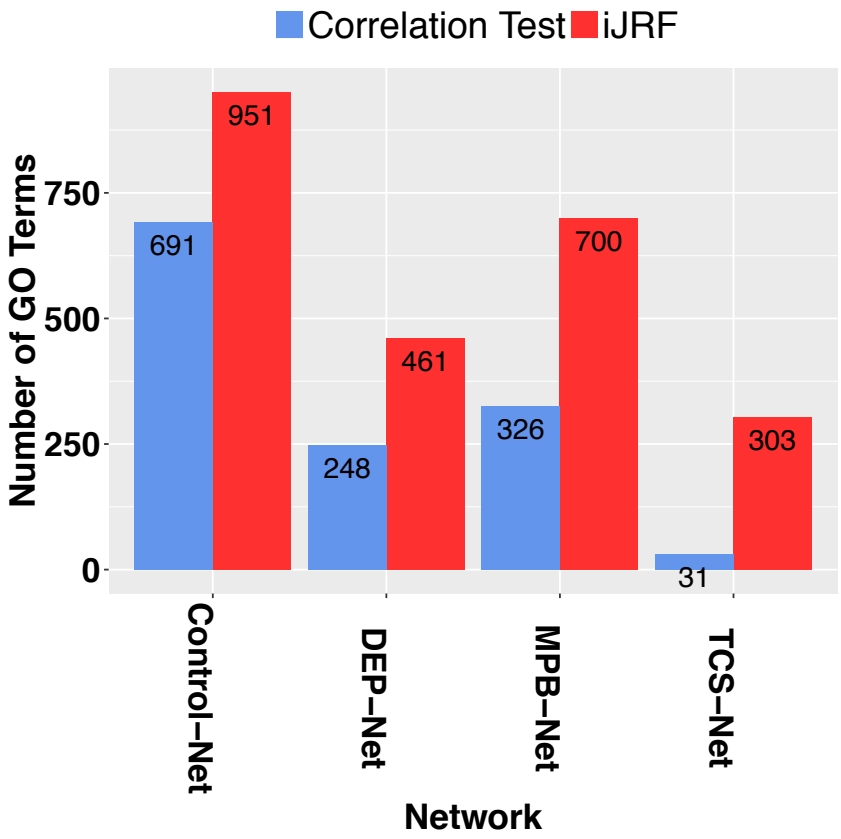


**Figure S6.** For each network (i.e., Control-Net, DEP-Net, MPB-Net, TCS-Net), we show the total number of enriched GO terms resulting from the correlation test (0.01 FDR cut-off) and iJRF. For each miRNA, we considered the set of connected messanger RNAs and derived the list of enriched GO terms. In particular, enrichment analysis was performed using David Tools (version 6.7) and only GO terms with Benjamini's adjusted p-value less than 0.01 were considered as enriched.

**(a) Correlation between miRNA-mRNA present only in Control-Net**

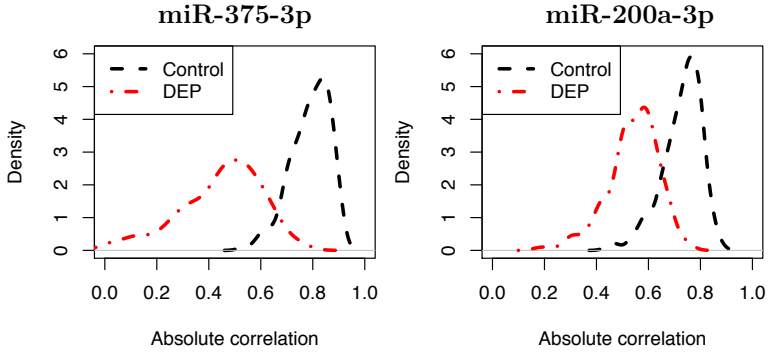


**(b) Test difference in correlation between DEP-Net and Control-Net**

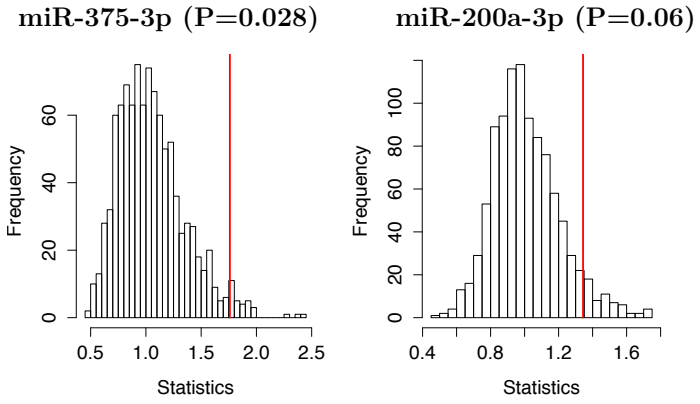


**Figure S7.** (a) Density of absolute correlation between miR-375-3p and miR-200a-3p with mRNAs connected only in Control-Net for DEP exposed data (red) and control data (black). (b) We test the difference in correlation between Control and DEP group for genes connected to miR-375-3p and miR-200a-3p only in Control-Net. For this purpose we consider the statistics $\frac{\sum_{j=1}|\rho_{j,m}^{Control}|}{\sum_{j=1}|\rho_{j,m}^{dep}|}$ with $\rho_{j,m}^{h}$ being the correlation between gene $j$ and miRNA $m$ under condition $h$. The test is performed using permutation techniques, permuting the label of samples between Control and DEP category. The histogram shows the null density of the statistics over 1,000 permutations while the red line shows the true value of the statistics.

**Table S2.** List of interactions contained in miRTarBase (Hsu *et al.*, 2010) for the top ten connected miRNAs in Control-Net. As shown, some of the interactions were contained in DEP-Net, MPB-Net and TCS-Net as well.

| miRNAs | mRNAs | DEP | MPB | TCS |
|---|---|---|---|---|
| miR-375 | HER2, TMTC4, SFT2D2 , KRT8 | | x | |
| miR-375 | PLAG1, CCDC88A, CELF2 | | | x |
| miR-375 | GATA6 | x | x | |
| miR-375 | CMTM4, FOLR1, CTSC | | | |
| miR-200a | ZEB2 | | | |
| miR-200a | HOXB5 | | | x |
| miR-200a | DLC1 | x | | |
| miR-150 | CBL | x | x | x |
| miR-150 | FOXK1 | | | |
| miR-150 | CCR6 | x | x | x |
| miR-342 | KCTD15 | x | | |
| miR-200b | FN1, DNMT3A | | x | |
| miR-200b | HOXB5 | | | x |
| miR-200b | DLC1 | x | | |
| miR-200b | CAB39 | x | | x |
| miR-204 | SOX4 | x | x | x |
| miR-204 | TRPM3 | x | | x |
| miR-429 | PARD6B | | | x |

# References


Cai, Y., Yan, X., Zhang, G., Zhao, W., and Jiao, S. (2016). Microrna-205 increases the sensitivity of docetaxel in breast cancer. *Oncology letters*, **11**(2), 1105–1109.

Chen, J., Shin, V. Y., Siu, M. T., Ho, J. C., Cheuk, I., and Kwong, A. (2016). mir-199a-5p confers tumor-suppressive role in triple-negative breast cancer. *BMC cancer*, **16**(1), 887.

Danaher, P., Wang, P., and Witten, D. M. (2014). The joint graphical lasso for inverse covariance estimation across multiple classes. *Journal of the Royal Statistical Society: Series B (Statistical Methodology)*, **76**(2), 373–397.

Das, S. and Lin, T. (2016). The role of micrornas in diagnosis, prognosis, metastasis and resistant cases in breast cancer. *Current pharmaceutical design*.

Hsu, S.-D., Lin, F.-M., Wu, W.-Y., Liang, C., Huang, W.-C., Chan, W.-L., Tsai, W.-T., Chen, G.-Z., Lee, C.-J., Chiu, C.-M., *et al.* (2010). mirtarbase: a database curates experimentally validated microrna–target interactions. *Nucleic acids research*, page gkq1107.

Huang, D. W., Sherman, B. T., and Lempicki, R. A. (2008). Systematic and integrative analysis of large gene lists using david bioinformatics resources. *Nature protocols*, **4**(1), 44–57.

Li, J., Lei, K., Wu, Z., Li, W., Liu, G., Liu, J., Cheng, F., and Tang, Y. (2016a). Network-based identification of micrornas as potential pharmacogenomic biomarkers for anticancer drugs. *Oncotarget*, **7**(29), 45584–45596.

Li, W., Wang, H., Zhang, J., Zhai, L., Chen, W., and Zhao, C. (2016b). mir-199a-5p regulates $\beta$1 integrin through ets-1 to suppress invasion in breast cancer. *Cancer science*, **107**(7), 916–923.

**Table S3.** Enriched categories for top 10 miRNAs in Control-Net. For each miRNA, we consider the list of genes connected in Control-Net but not in chemical networks and derive enriched GO terms using David Tools. For each pathway, we report Benjamini adjusted p-value. Only pathways with Benjamini adjusted p-values smaller than 0.01 are shown.

| miRNA | Pathways enriched for genes connected to miRNA in Control-Net but not in DEP-Net. |
|---|---|
| miR-146b-5p | Phosphoprotein (4E-3), Bicellular tight junction (8E-3), Cell junction (9E-3) |
| miR-200a-3p | Plasma Membrane (1E-10), Cell-Cell Junction (2E-5), Gland Development (2E-4), Skeletal System Development (2E-3), Regulation of Cell Proliferation (3E-3), Biological Adhesion (6E-3) |
| miR-429 | Plasma Membrane (1E-13), Homeostatic Process (4E-7), chemical homeostasis (4E-7),ion Homeostasis (2E-4) Cell adhesion (4E-4), Gland development (1E-3), regulation of cell proliferation (6E-3), lipid binding (7E-3) |
| miR-150-5p | plasma membrane (2E-4), ntracellular signaling cascade (2E-3), external side of plasma membrane (9E-3) |
| miR-342-3p | plasma membrane (3E-4), external side of plasma membrane (5E-3) |
| miR-200b-3p | plasma membrane (1E-11), gland development (10E-6), apical junction complex (5E-4), mammary gland development (6E-3), cell adhesion (8E-3), biological adhesion (8E-3), cell-cell junction (6E-3) |
| miR-204-5p | plasma membrane (9E-17), chemical homeostasis (6E-5), cell-cell junction (5E-5), ion homeostasis (3E-4), homeostatic process (4E-4) , apical junction complex (5E-4), cellular chemical homeostasis (7E-4) |
| miR-483-3p | Plasma Membrane (3E-12), response to hormone stimulus (10E-7), response to endogenous stimulus (3E-6), response to organic substance (7E-6), regulation of cell proliferation (7E-4), gland development (2E-3), calcium ion binding (2E-3), response to drug (4E-3), lipid binding (9E-3) |
| miR-375-3p | Gland Development (1E-7), gland morphogenesis (1E-5), plasma membrane (2E-5) epithelium development (7E-4) |
| miR-214-3p | Gland Morphogenesis (6E-4), Response to Organic Substance (1E-3), Plasma Membrane (3E-3) |

| miRNA | Pathways enriched for genes connected to miRNA in Control-Net but not in MPB-Net. |
|---|---|
| miR-146b-5p | Plasma Membrane (9E-4) |
| miR-429 | Plasma Membrane (5E-5) |
| miR-150-5p | Intracellular Signaling Cascade (2E-3), Guanyl ribonucleotide Binding (4E-3), Positive Regulation of Macromolecule Metabolic Process (5E-3) |
| miR-200b-3p | Membrane (8E-3) |
| miR-204-5p | Plasma Membrane (3E-7), Chemical Homeostasis (7E-3), Gland Development (8E-3), Ion Homeostasis (9E-3) |
| miR-483-3p | Plasma Membrane (2E-7), Lipid Binding (2E-3) , response to hormone stimulus (2E-3) response to organic substance (6E-3) |
| miR-375-3p | gland development (1E-3) |

| miRNA | Pathways enriched for genes connected to miRNA in Control-Net but not in TCS-Net |
|---|---|
| miR-146b-5p | Phosphoprotein (3E-3) |
| miR-200a-3p | apical plasma membrane (5E-6), basolateral plasma membrane (6E-4), cell surface (9E-4), tricellular tight junction (1E-3), extracellular exosome (4E-3) |
| miR-429 | apical plasma membrane (4E-6), response to progesterone (8E-4), cell adhesion (5E-3) protein binding (8E-3), microvillus (2E-3), extracellular exosome (5E-3) |
| miR-150-5p | Cell activation (7E-14), leukocyte activation (9E-14), positive regulation of immune system process (2E-13) immune response (4E-13), T cell activation (3E-11), lymphocyte activation (5E-11), intracellular signaling cascade (1E-8), regulation of cell activation (2E-8), plasma membrane (2E-8), positive regulation of immune response (3E-8), regulation of cytokine production (1E-6), positive regulation of response to stimulus (3E-6), cell receptor signaling pathway (3E-6) |
| miR-342-3p | External Side of Plasma Membrane (7E-11), Positive Regulation of GTPase Activity (1E-8) Intracellular Signal Transduction (4E-8), Inflammatory Response (2E-7), Immune Response (3E-5) Cytoskeleton (1E-5), Positive Regulation of ERK1 and ERK2 Cascade (2E-4), T Cell Differentiation (5E-4) |
| miR-200b-3p | plasma membrane (7E-9), gland development (9E-4) |
| miR-204-5p | plasma membrane (6E-15), ion homeostasis (6E-5), chemical homeostasis (2E-4), cellular ion homeostasis (5E-4), cellular chemical homeostasis (7E-4), apical part of cell (1E-3), homeostatic process (2E-3) |
| miR-483-3p | plasma membrane (1E-12), response to hormone stimulus (5E-5), response to organic substance (5E-4) regulation of cell proliferation (1E-3) , anchoring junction (2E-3), gland development (6E-3) response to oxygen levels (7E-3), tissue remodeling (8E-3), adherens junction (7E-3) |

Petralia, F., Song, W.-M., Tu, Z., and Wang, P. (2016). New method for joint network analysis reveals common and different coexpression patterns among genes and proteins in breast cancer. *Journal of Proteome Research*, **15**(3), 743–754. PMID: 26733076.

Shin, V., Siu, J., Cheuk, I., Ng, E., and Kwong, A. (2015). Circulating cell-free mirnas as biomarker for triple-negative breast cancer. *British journal of cancer*, **112**(11), 1751–1759.

Tusher, V. G., Tibshirani, R., and Chu, G. (2001). Significance analysis of microarrays applied to the ionizing radiation response. *Proceedings of the National Academy of Sciences*, **98**(9), 5116–5121.

Yi, H., Liang, B., Jia, J., Liang, N., Xu, H., Ju, G., Ma, S., and Liu, X. (2013). Differential roles of mir-199a-5p in radiation-induced autophagy in breast cancer cells. *FEBS letters*, **587**(5), 436–443.

Zhang, H., Li, B., Zhao, H., and Chang, J. (2015). The expression and clinical significance of serum mir-205 for breast cancer and its role in detection of human cancers. *International journal of clinical and experimental medicine*, **8**(2), 3034.